

# 1 Upper Ocean Response on the Passage of Tropical Cyclones in 2 the Azores Region

3 Miguel M. Lima<sup>1</sup>, Célia M. Gouveia<sup>1,2</sup>, Ricardo M. Trigo<sup>1,3</sup>

4 *Correspondence to:* Miguel M. Lima

5 <sup>1</sup>Instituto Dom Luiz (IDL), Faculdade de Ciências, Universidade de Lisboa, 1749-016, Lisboa, Portugal

6 <sup>2</sup>Instituto Português do Mar e da Atmosfera (IPMA), I.P., 1749-077, Rua C do Aeroporto, Lisboa, Portugal

7 <sup>3</sup>Departamento de Meteorologia, Universidade Federal do Rio de Janeiro, Rio de Janeiro 21941-919, Brasil

8 **Abstract.** Tropical Cyclones (TCs) are extreme climate events that are known to strongly interact with the ocean  
9 through two mechanisms: dynamically through the associated intense wind stress, and thermodynamically through  
10 moist enthalpy exchanges at the ocean surface. These interactions contribute to relevant oceanic responses during and  
11 after the passage of a TC, namely the induction of a cold wake and the production of chlorophyll (Chl-a) blooms. This  
12 study aimed to understand these interactions in the Azores region, an area with relatively low cyclonic activity for the  
13 North Atlantic basin, since the area experiences much less intense events than the rest of the basin. Results for the  
14 1998-2020 period showed that the averaged induced anomalies were on the order of  $+0.050 \text{ mg m}^{-3}$  for the Chl-a and  
15  $-1.615 \text{ K}^{\circ}\text{C}$  for SST. Furthermore, looking at the role played by several TCs characteristics we found that the intensity  
16 of the TCs was the most important condition for the development of upper ocean responses. Additionally, it was found  
17 that bigger TCs ~~induced~~caused greater induced anomalies in both variables, while faster ones created greater Chl-a  
18 responses, and TCs that occurred later in the season had greater TC-related anomalies. Two case studies (Ophelia, in  
19 2017, and Nadine, in 2012) were conducted to better understand each upper ocean response. Ophelia showed to affect  
20 the SST at an earlier stage while the biggest Chl-a induced anomalies were registered at a later stage, allowing the  
21 conclusion that thermodynamic exchanges conditioned the SST more while dynamical mixing might have played a  
22 more important role in the later stage. Nadine showed the importance of the TC track geometry, revealing that the TC  
23 track observed in each event can impact a specific region for longer, and therefore ~~induce~~greater induced anomalies.

## 24 Introduction

25 Tropical Cyclones (TCs) are potentially intense atmospheric disturbances which are characterised by a low-pressure  
26 centre (eye) where strong winds curl around. Among other important properties, TCs are thermodynamic dependent  
27 phenomena, meaning that intense temperature gradients need to occur in the lower atmosphere to maintain and  
28 intensify the storm. Thus, TCs are fed from warm sea water which provide a strong moist enthalpy flux from the  
29 oceanic surface to maintain a steep temperature gradient within the lower and middle troposphere and produce massive  
30 water vapour convection (Emanuel, 2003; Holton and Hakim, 2012; Pearce, 1987).

31 The strong wind stress present near the surface and the associated intense curl are also shown to induce vertical mixing  
32 and Ekman upwelling in the upper layer of the ocean. In his seminal study, Price (1981) shows, through both observed  
33 and numerical modelling data, the evolution of sea surface temperature (SST) on the passage of a hurricane, with the  
34 emergence of a cold wake of SST after a TC due to entrainment of water from ~~shallow~~ deeper layers. This effect has  
35 since been well studied and documented with many case studies observed, for example, the case of Hurricane Felix,  
36 in the vicinity of Bermuda in 1995, that showed decreases in the order of 3.5-4 °C (Dickey *et al.*, 1998), or the cases  
37 of cyclones Nargis (2008) and Laila (2010), in the Bay of Bengal, that caused SSTs to drop by around 1.76 °C  
38 (Maneesha *et al.*, 2012). Additionally, several model-based works focused on either the effects caused by the TCs, or  
39 the interaction of the TC with its own cold wake (e.g., Chen *et al.*, 2017; Zhang *et al.*, 2019).

40 There are also biological responses to the passage of a TC. Due to the upwelling of colder water, transport of nutrient-  
41 rich water from the sub-superficial layer may also occur (Kawai and Wada, 2011). In this case, phytoplankton can  
42 quickly increase in the surface layer following the rise in nutrients. This increase can be remotely sensed through  
43 satellite observations that capture the chlorophyll-a concentration (Chl-a) increasing after the passage of a TC, since  
44 Chl-a is generally accepted as a proxy for biological activity (Kawai and Wada, 2011; Liu *et al.*, 2009; Subrahmanyam  
45 *et al.*, 2002; Walker *et al.*, 2005).

46 The oceanic response, either physical or biological, to the passage of a TC depends on various aspects, most  
47 remarkably the TC's intensity and its translation speed but also the oceanic subsurface conditions (Zheng *et al.*, 2008).  
48 The magnitude and significance of these aspects on the modulation of the oceanic response ~~varies~~ vary regionally,  
49 although it is generally regarded that the most impactful phenomena ~~to be those of an~~ are intense and slow ~~TC~~ TCs  
50 (Chacko, 2019; Price, 1981; Price *et al.*, 1994). Recent studies (e.g., Chacko, 2019; Pan *et al.*, 2018; Shropshire *et al.*,  
51 2016) have shown that regional differences do matter when studying the biological response. In the case of the Bay  
52 of Bengal, it was shown that the intensity of a TC is less important, and the most meaningful aspects are the TC's  
53 translation speed and, to a lesser degree, a pre-existing shallow mixed layer (Chacko 2019). The results from this study  
54 are important to stress that relatively weaker TCs can also induce a strong biological response after their passage.

55 Until now, the Azores region has not been studied regarding its thermodynamic and biological impacts. This section  
56 of the North Atlantic basin presents much fewer and weaker cyclones than the tropical band of the basin, with this  
57 region being mainly a zone where TCs undergo either cyclosis or post-tropical transition into extra-tropical cyclones  
58 or mid-latitude storms (Baatsen *et al.*, 2015; Haarsma *et al.*, 2013). The north-eastern Atlantic (NEA) basin, where the  
59 Azores archipelago is located, presents significantly less TCs than the western counterpart, closer to the USA coast  
60 (Baatsen *et al.*, 2015; Lima *et al.*, 2021; Haarsma *et al.*, 2013). However, there is growing evidence of a significant  
61 increase in the frequency of strong TCs in both western (Kossin *et al.*, 2020) and eastern (Lima *et al.*, 2021) halves of  
62 the north Atlantic Ocean. The climatology of the area points to a south-north gradient in both SST and Chl-a, with a  
63 decrease in the former and an increase in the latter (Amorim *et al.*, 2017; Caldeira and Reis, 2017). In general, the  
64 southern part of the Azores region offers SSTs high enough to maintain TCs, although the necessary atmospheric  
65 conditions (e.g., high lapse rates and low wind shear) need to occur for their passage northeast through the Azores

66 (Lima et al., 2021). However, this area is undergoing a transition due to anthropogenic climate change and an increase  
67 both in number and intensity of TCs is expected (Baatsen et al., 2015; Haarsma et al., 2013). Therefore, the NEA basin  
68 is a challenging study region to assess the impact that lower intensity TCs have on the oceanic surface.

69 The main aim of this study is to analyse in detail the upper ocean response observed after the passage of a TC in the  
70 Azores region, which is characterised by its lower-than-normal cyclonic activity in relation to the rest of the north  
71 Atlantic basin. In particular, we aim to evaluate the impacts on SST and Chl-a concentration produced by important  
72 TC characteristics (averaged maximum wind speed, average translation speed, overall impacted area, time of  
73 occurrence, and geometry of the track). Two practical case studies, relative to Nadine (2012) and Ophelia (2017) are  
74 then thoroughly analysed to reflect the drawn conclusions for this area.

## 75 **Data**

76 The main data used to evaluate the oceanic response in this study is divided into three main parts: Remotely sensed  
77 interpolated data used to characterise the Chl-a and SST, respectively, and TC track data, which provides the necessary  
78 additional information on the location and dynamic variables of each TC, that allow to explore the oceanic response  
79 in the aforementioned data. Additionally, non-interpolated datasets are used for the case studies to validate the  
80 interpolated ones; and wind-stress data is used for the Hurricane Ophelia study case.

81 Biological oceanic response was evaluated using a multi-sensor daily Chl-a product available through the Copernicus  
82 Marine Environment Monitoring Service (CMEMS) in a 4 km x 4 km resolution from the end of 1997 to the present  
83 (CMEMS, 2021b). This product, delivered by the ACRI-ST company, is based on the Copernicus-GlobColour project  
84 and obtained by merging different sensors: SeaWiFS, MODIS, MERIS, VIIRS-SNPP&JPSS1, OLCI-S3A&S3B. The  
85 final Chl-a product is a mix of several algorithms that consider different water conditions, such as oligotrophic,  
86 mesotrophic, coastal, clear, and complex waters (Garnesson et al., 2019). To produce a “cloud free” product, the  
87 resulting data was subjected to daily interpolation to fill any gaps (Krasnopolsky et al., 2016; Saulquin et al., 2019).  
88 The lack of gaps in this dataset is particularly relevant in the context of this study since the areas analysed will be  
89 concentrated around the TCs; it is then expected that large amounts of the analysed areas would be under cloud  
90 coverage and, therefore, some of the analysed data is not real but interpolated values. Nonetheless, CMEMS provides  
91 approximate uncertainty levels for this data, which we used to assess the quality of our results. For further validation  
92 purposes we used also a non-interpolated Chl-a product generated by the Ocean Colour component of the European  
93 Space Agency’s Climate Change Initiative project (OC-CCI) (Sathyendranath et al., 2019). This dataset results from  
94 a merge of several sensors: SeaWiFS LAC and GAC, MODIS Aqua, MERIS, VIIRS, and OLCI. ESA’s OCC-CI  
95 version 5.0 Chl-a product has 0.042° resolution and a daily temporal resolution (Sathyendranath et al., 2021).

96 To evaluate the physical oceanic response and to relate this to the biological one, a daily SST dataset from the CMEMS  
97 was used, with a 0.05° resolution. This data is available from 1981 up to the near present (CMEMS, 2021a). Similarly,  
98 to the previous CMEMS interpolated Chl-a product, the SST field is also a blended gap-free analysis product, with  
99 the present one resulting from re-processed (A)ATSR, SLSTR and AVHRR sensor data being applied to the

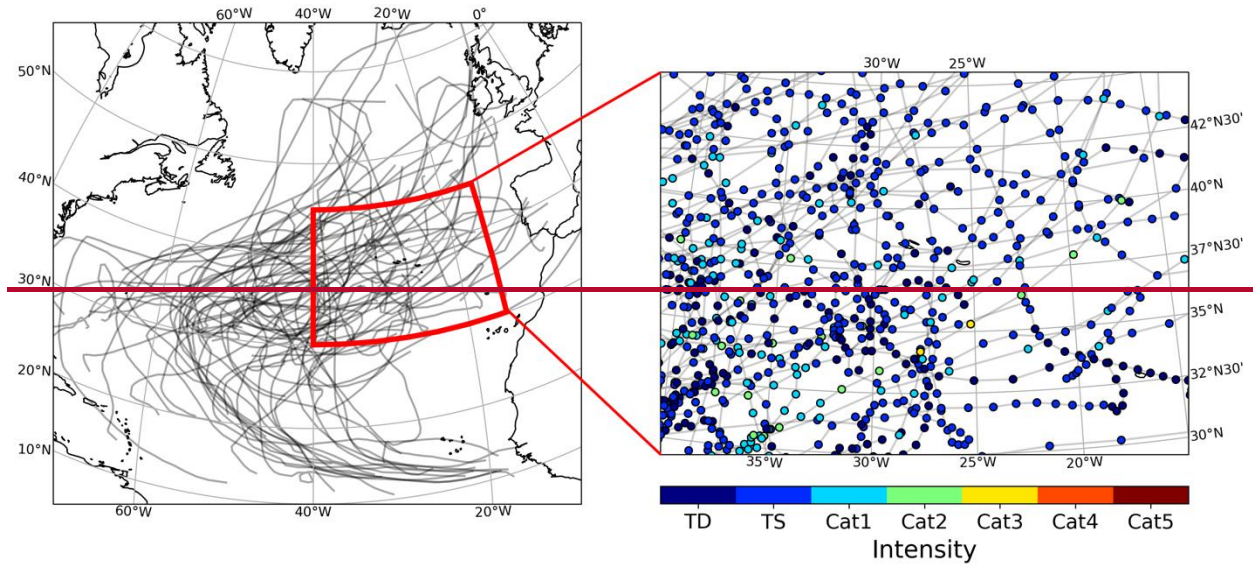
100 Operational SST and Sea Ice Analysis (OSTIA) system (Donlon et al., 2012). This reprocessed analysis product  
101 provides an estimate of the SST at 20 cm depth. The inputs to the system are SSTs at 10:30 am and 10.30 pm local  
102 time which means that the analyses roughly correspond to the daily average SST (Good et al., 2020; Lavergne et al.,  
103 2019; Merchant et al., 2013). As stated before, approximated error values for SST are also provided by CMEMS.  
104 Additionally, AVHRR Pathfinder version 5.3 collated data was used as non-interpolated data for validation. This  
105 dataset, similarly to the CMEMS one, is a collection of twice-daily (averaged to daily), ~~4km~~4 km spatial resolution,  
106 merged SST product, provided by NOAA's National Centers for Environmental Information (Saha et al., 2018). The  
107 merge of this data, however, is only used to spatially collate the data, as it is a single instrument measurement  
108 (AVHRR) onboard NOAA-7 through NOAA-19 Polar Operational Environmental Satellites (POES).

109 Wind stress data to assist in the analysis of the Hurricane Ophelia study case was provided by NOAA's CoastWatch  
110 dataset available at [https://coastwatch.pfeg.noaa.gov/erddap/griddap/erdQMstress1day\\_LonPM180.html](https://coastwatch.pfeg.noaa.gov/erddap/griddap/erdQMstress1day_LonPM180.html). This dataset  
111 is derived from wind measurements obtained from the Advanced Scatterometer (ASCAT) instrument on board  
112 EUMETSAT's MetOp satellites (A and B) at a daily 0.25° resolution, from 2013 to the present. ASCAT presents a  
113 near all-weather capacity (not affected by clouds), as it operates a frequency in C-band (5.255 GHz), therefore,  
114 minimizing the number of missing values in predominately clouded areas such as the case of TC paths.

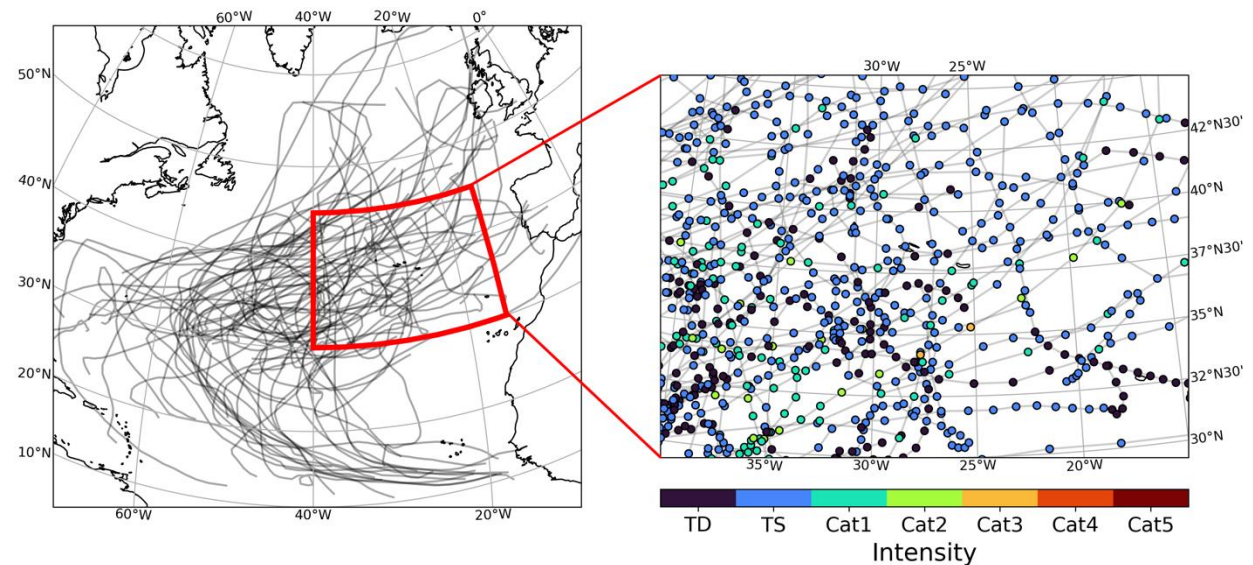
115 The TC track data is made available by the *International Best Track Archive for Climate Stewardship Project* version  
116 4 (IBTrACS v4) free access dataset (Knapp *et al.*, 2009). This dataset contains global information regarding TC  
117 activity since the 1851 hurricane season up to 2020. It aggregates variables such as TC geographical location,  
118 maximum wind speed, minimum sea level pressure, and storm radius estimation based on wind intensity, measured at  
119 6-hour intervals (original dataset interpolates for increased resolution, at 3-hour rates, however this interpolation only  
120 includes the geographical location). For the 1998-2020 period, the Azores region experienced the passage of 62  
121 individual TCs accounting to 642 6-hour observations that are categorised in the following intensities according to the  
122 Saffir-Simpson hurricane wind scale (Taylor *et al.*, 2010):

- 123 ● 148 tropical depression observations.
- 124 ● 389 tropical storm observations.
- 125 ● 85 category 1 hurricane observations.
- 126 ● 18 category 2 hurricane observations.
- 127 ● 2 category 3 hurricane observations.

128 The full TC tracks can be better visualised in Fig. 1, with the left panel showing the full track for all these 62 ~~TCs~~TCs  
129 observed in the NA basin for the 1998-2020 period and the right panel showing a zoomed view relative to the  
130 considered Azores region. Tropical depression observations (dark blue in Fig. 1, right panel) account for 23 % of the  
131 total observations and will not be considered in this study, as they present the lower branch of intensities with winds  
132 below the 34-kt (18 m/s) threshold. Therefore, a total of 494 TC 6-hour observations were considered for this study.



133



134

135 **Figure 1 - Left panel: North Atlantic basin and the tracks for of all the TCs that went through or occurred inside the study**  
 136 **region (shown by the red outline). Right panel: Zoom of the previous red outline, with each TC observation marked in**  
 137 **different colours for intensity (TD: Tropical Depression; TS: Tropical Storm; Cat1 - Cat5: Hurricane category according**  
 138 **to the hurricane Saffir-Simpson wind scale).**

139 Since the interpolated datasets used for most of this study do not share the same time frame and to better encapsulate  
 140 full years of data, the timeframe of the present study will be from January 1st of 1998 to December 31st of 2020.  
 141 Moreover, while we have extracted all the data described above covering the entire North Atlantic basin, we will focus  
 142 on the area around the Azores archipelago, delimited by the 15°W15° W and 40°W40° W meridians and between the  
 143 30°N30° N and the 45° parallels (Fig. 1).

## 144 **Methodology**

145 The region of study was chosen due to its nature regarding TCs, since it is an area with fewer and less intense tropical  
146 storms (Hart and Evans, 2001; Lima et al., 2021; Ramsay, 2017). Generally, tropical cyclosis and post-tropical  
147 transition occur here (Baatsen et al., 2015; Haarsma et al., 2013). Because of these aspects, it corresponds to a much  
148 less studied area and is a good region to characterise oceanic biophysical effects after the passage of (generally) weaker  
149 TCs at higher-than-tropical latitudes and to compare the obtained results with previous literature.

150 To cope with large amounts of data, the bio-physical response was evaluated within a small area around individual  
151 locations obtained for each TCs' best-track location. For this, we used the approximated quadrant radius given by the  
152 IBTrACS v4 dataset. This dataset provides different types of radii depending on the considered isotach, for this study  
153 we used the 34-kt isotach as it corresponds to the lower-bound for the Tropical Storm status according to the Saffir-  
154 Simpson hurricane wind scale (Taylor et al., 2010). Since the considered area of analysis falls above the 34-kt isotach,  
155 tropical depressions were not considered (exact partition of intensities is given at the beginning of the *Results* section).  
156 There are some missing radii values in the middle of TC tracks and ~~in order~~, to correct those, a simple linear regression  
157 was applied. To illustrate the application of this methodology we present the study cases in the *results and discussion*  
158 section, for hurricanes Ophelia (2017) and Nadine (2012). From inside this area of analysis, we may retrieve the Chl-  
159 a concentration and SST at their respective resolution. The analysis inside the considered area was performed using  
160 histograms, in which each pixel inside the 34-kt isotach contributes to that TCs histogram.

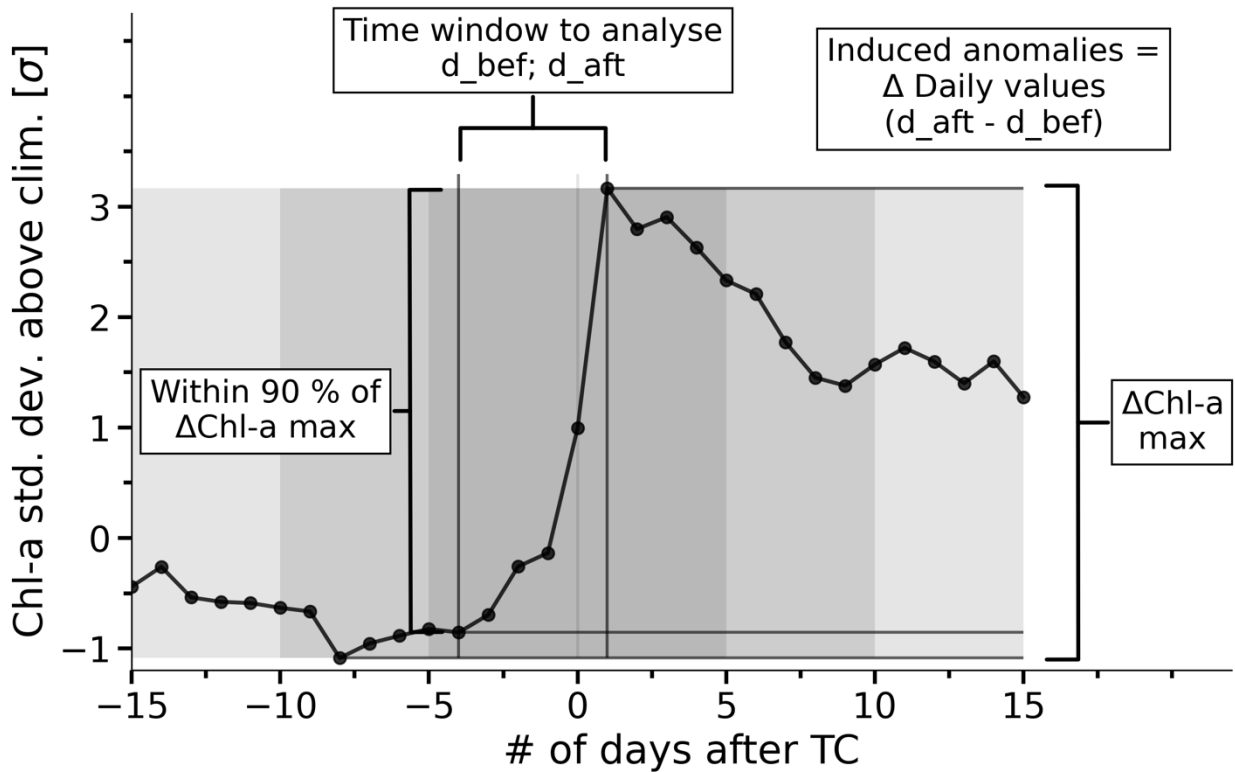
161 To analyse the TCs' impact on their passage, inspiration was taken from Kawai and Wada (2011), who computed the  
162 climatic monthly standard deviation of Chl-a on 0.25° grids over a 5-year study period. Here, we ~~computed for each~~  
163 ~~storm~~ compute the daily normalized anomaly from the climatological value (in standard deviation units). For this, we  
164 first calculated the climatological mean and associated standard deviation of both Chl-a and SST ~~over their respective~~  
165 ~~grids relative to the climatology over~~ values for the region that is impacted by each TC on the day of analysis. This is  
166 achieved considering the 3 days before and 3 days after the day of analysis, totalling one week that is then retrieved  
167 from the entire study period of 22 years, thus ensuring a larger sample and a smoother continuous curve. Then, we  
168 compute the mean value in the same area (in which only the TC area impacted by the TC was considered) for the  
169 ~~study's complete time frame; this~~ day of analysis, and finally, we calculate the normalized anomaly from the  
170 climatology on that day. This analysis was performed considering 30 days before and after each TC to allow then the  
171 analysis and identification of an ideal window to compute the induced anomalies. To compute this ideal window, we  
172 searched for the maximum difference between the number of standard deviations over the climatological value before  
173 and after the storm.

174 To compromise between having the maximum difference and ensuring a time window as close as possible to the storm  
175 (to minimize external factors to the TC), we performed a sensibility study on the length and location of the considered  
176 time window. First, we analyse the overall maximum difference in the 61-day period (including the day of the storm)  
177 and then search for a secondary maximum value that is within 10\_% of it considering a smaller sample of days,  
178 decreasing in groups of 5 days each time this search is made (e.g., the first iteration would be 25 days before and 30  
179 after, the second 30 before and 25 after, the third 25 before and after, etc.), until an optimum maximum difference

180 value is identified. With this window defined, the induced (or TC-related) anomalies are simply the difference between  
181 the daily values of Chl-a or SST after and before the TC.

182 As an example of this methodology, Fig. 2 shows the Chl-a standard deviation over the climatological value in the  
183 case of Hurricane Nadine. In this case, only 15 days around the TC are shown for clarity. We can see that the maximum  
184 difference is obtained between 8 days before and 1 day after the storm ( $\Delta\text{Chl-a max}$ ). However, when we take into  
185 account the compromise of considering windows located as close as possible to the occurrence of the TC over the  
186 region, we see that the value found between 4 days before and 1 day after is within 10% of the absolute maximum.  
187 This methodology is then applied to all 6-hour observations individually and for each TC, thus resulting in two groups  
188 of induced anomalies (per TC and per 6-hour observations) where we can study these with respect to the TCs averaged  
189 (per TC) or instantaneous (6-observations) characteristics.

190 To address the possibility that some pixels are overlaid on top of each other, which would contaminate the analysis,  
191 as observed in the case of the slow erratic Hurricane Nadine (presented in the *results and discussion* section as a study  
192 case), we did not take into consideration the days in which the TC is over the aforementioned overlaid region. In [the](#)  
193 [case of](#) these [cases pixels](#), the [days](#) considered [are those when to be after](#) the TC [is the day after it](#) has completely  
194 [travelled passed](#) over the area (i.e., [the observations in](#) that pixel [is no longer inside the radius of influence of](#) [during](#)  
195 [the days](#) the TC [is still over the area are discarded](#)). However, when we consider independent 6-hour observations,  
196 this caveat cannot be accounted for since we have no way of knowing if that area has been influenced or not by the  
197 TC before, for how long, or even if a future observation will impact the area.



199 **Figure 2 - Schematic of the applied methodology for each TC. Black line shows the number of standard deviations from the**  
200 **climatological values for the area surrounding Hurricane Nadine. A detailed description of this methodology can be found**  
201 **in the text.**

202 As previously mentioned in the *Data* section, the interpolated data used for this study is expected to encounter some  
203 regions where clouds are to be expected due to the presence of the TCs. To account for this potential caveat, we looked  
204 at the uncertainties associated with the data before and after the TCs, as well as during the TC (e.g., day 0 in Fig. 2),  
205 to evaluate if there were clear increases in uncertainty for cloud covered situations.

206 Two case studies were looked at in greater detail: Hurricane Ophelia (2017) and Hurricane Nadine (2012). The former  
207 was performed to assess the different impacts along the lifecycle of the storm, and different histograms were produced  
208 for smaller portions of the TC. The latter was made to analyse the possible increasing impacts the storm geometry  
209 could cause. Additionally, these study cases were used as validation for the interpolated “cloud-free” data, where a  
210 comparison was made between the non-interpolated and the interpolated “cloud-free” data described in the *Data*  
211 section.

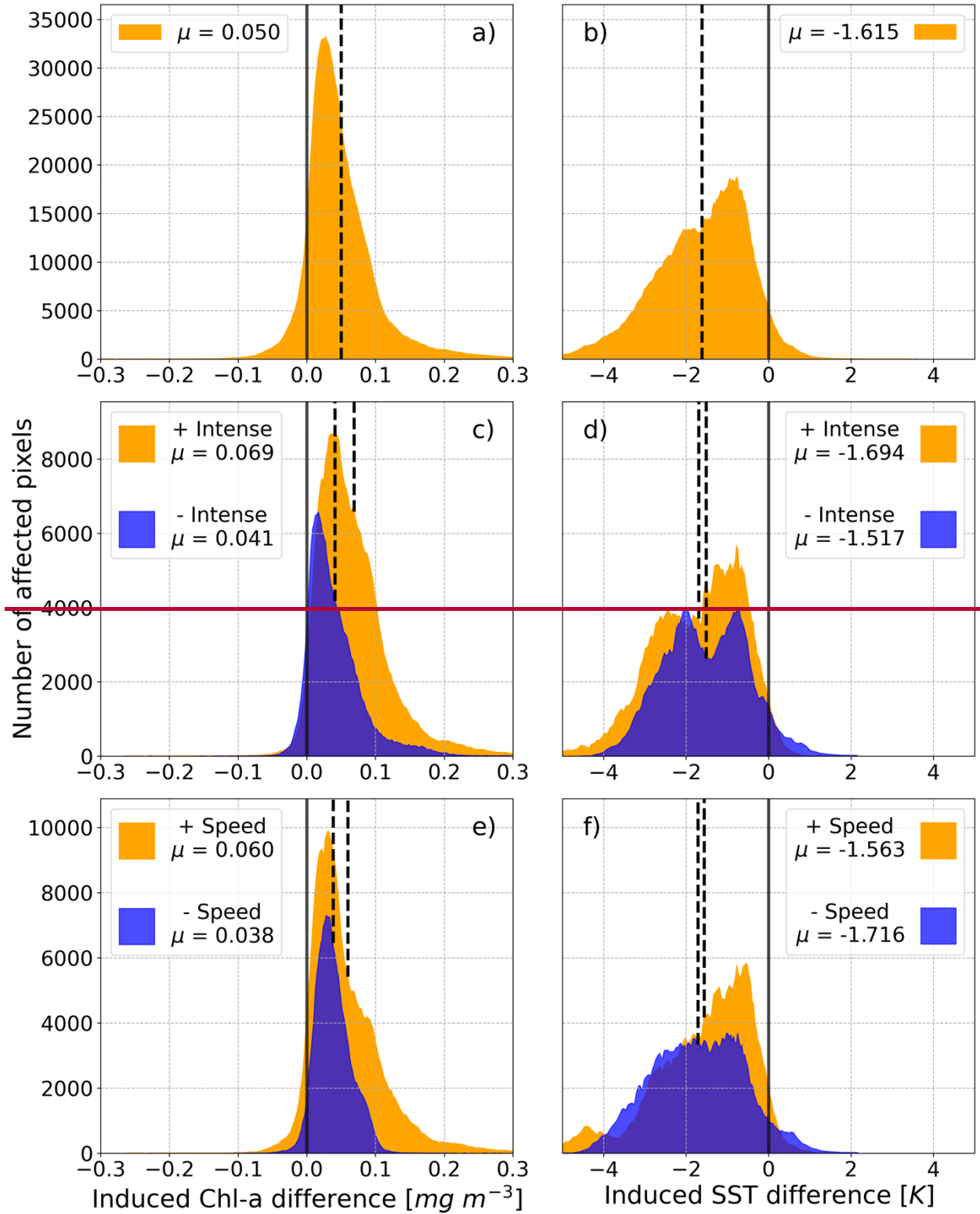
## 212 **Results and Discussion**

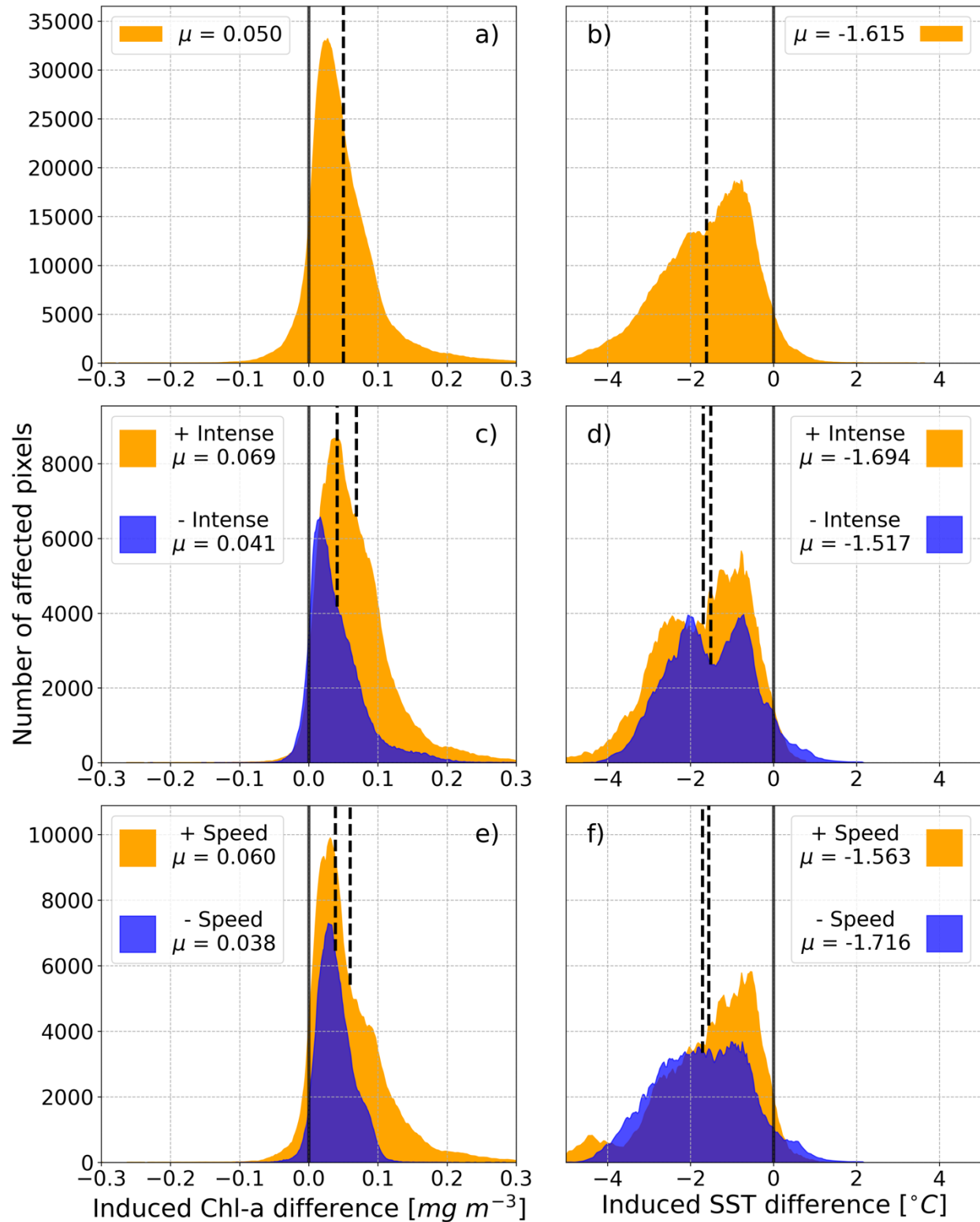
213 Applying the mentioned methodology leaves us with a large pool of induced anomalies, from which we can now  
214 evaluate the distribution of [these TC-related](#) anomalies for both the Chl-a and SST as shown in Figs. 3a and 3b in the  
215 form of histograms of induced Chl-a and SST [induced](#) anomalies, respectively. Both variables present a large impact  
216 after the passage of TCs, with the Chl-a presenting a mean response of positive  $0.050 \text{ mg m}^{-3}$  and the SST showing a  
217 mean response of ~~negative~~  $-1.615 \text{ K}^{\circ}\text{C}$ . Figs. 3c-f show the corresponding distributions as a function of the cyclone’s  
218 intensities (Figs. 3c and 3d) and translation speeds (Figs. 3e and 3f). To make these distinctions, we chose only the  
219 high values (either regarding intensity or translation speed) to be those above the third quartile and the lower values  
220 to be those below the second quartile.

221 Firstly, regarding intensity (Figs. 3c and 3d), we have the induced response of the most powerful intensities in orange  
222 and the weaker ones in blue. Regarding the impact as a function of intensity it is possible to observe that more powerful  
223 TCs tend to induce a stronger biological response than weaker ones, which have a mean response closer to zero. It is  
224 also important to note that the more powerful TCs have a response that is much more skewed towards extreme positive  
225 values of Chl-a. Fig. 3d also shows a great impact regarding different intensities in SST, in which even weaker TCs  
226 show a substantial mean response of  $-1.517 \text{ K}^{\circ}\text{C}$  and nearly all the analysed pixels showing negative induced  
227 anomalies. Important to note the nearly bimodal nature of this distribution, which can be attributed to both the earlier  
228 phase of TCs (more energy being drawn from the ocean) resulting in more negative SST values, and the less negative  
229 corresponding to the later part of TCs since baroclinic instabilities are more prevalent than the action of moist enthalpy  
230 flux from the ocean at this phase (Baatsen et al., 2015; Emanuel, 2003). Powerful TCs induced a more varied  
231 distribution of [induced](#) anomalies, with a mean response of  $-1.694 \text{ K}^{\circ}\text{C}$ .



232 Regarding the different translation speeds, Fig. 3e shows that, for biological responses, faster TCs show a greater  
233 mean value of  $+0.060 \text{ mg m}^{-3}$ . This difference is not as ~~expressive~~remarkable as the one in Fig. 3c. On the other hand,  
234 the SST response (Fig. 3f) seems to be weakly impacted by the TC's translation speed, with slower TCs ~~have~~having  
235 a slightly stronger impact than faster ones, while the mean response values do not differ as much as the ones in Fig.  
236 3d. Additionally, even if faster TCs do not affect the SST response as much as slower ones, the mean value is still  
237 close to what is seen in the general case in Fig. 3b, and most of the impact is towards negative SSTs.





239

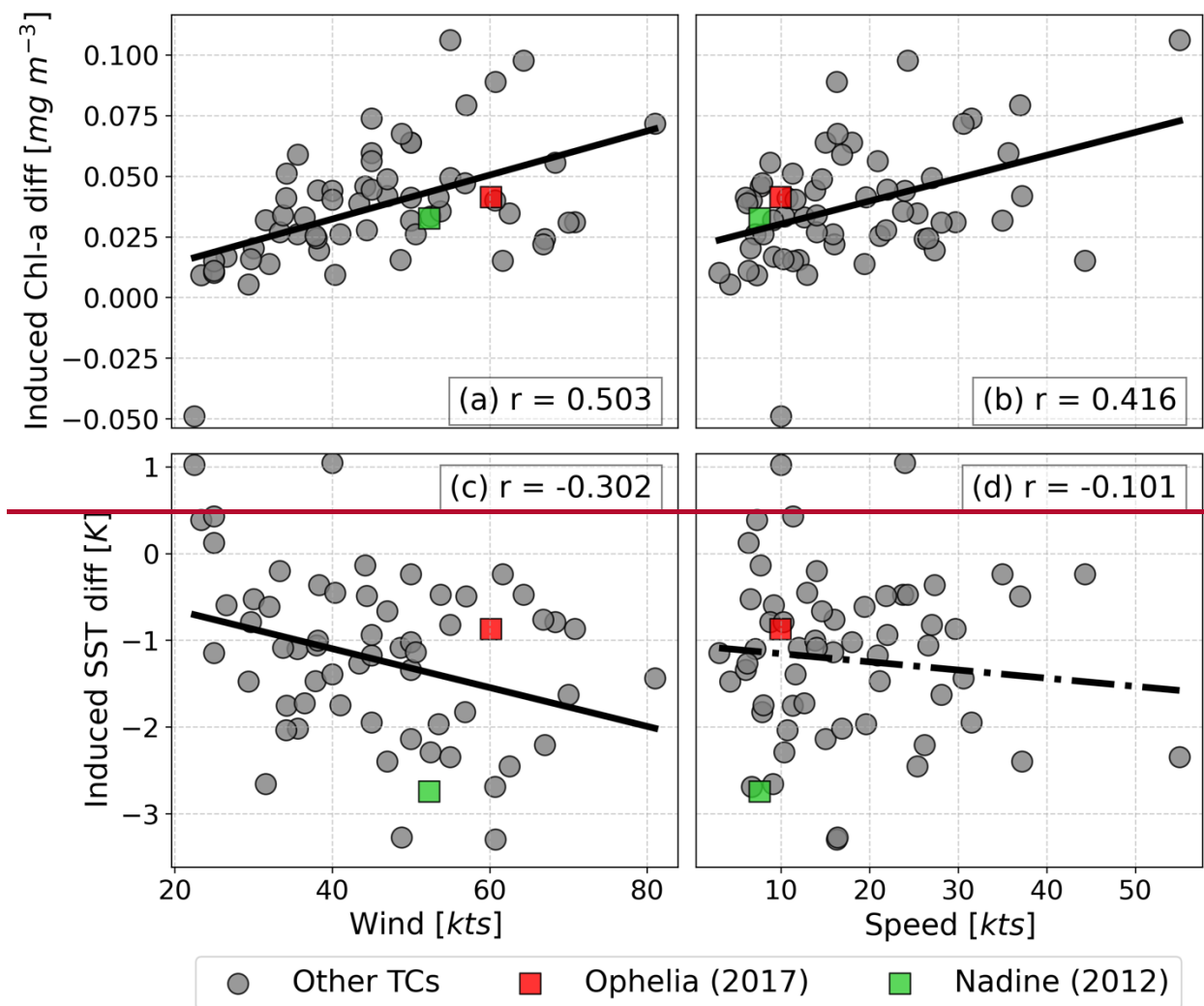
240

241

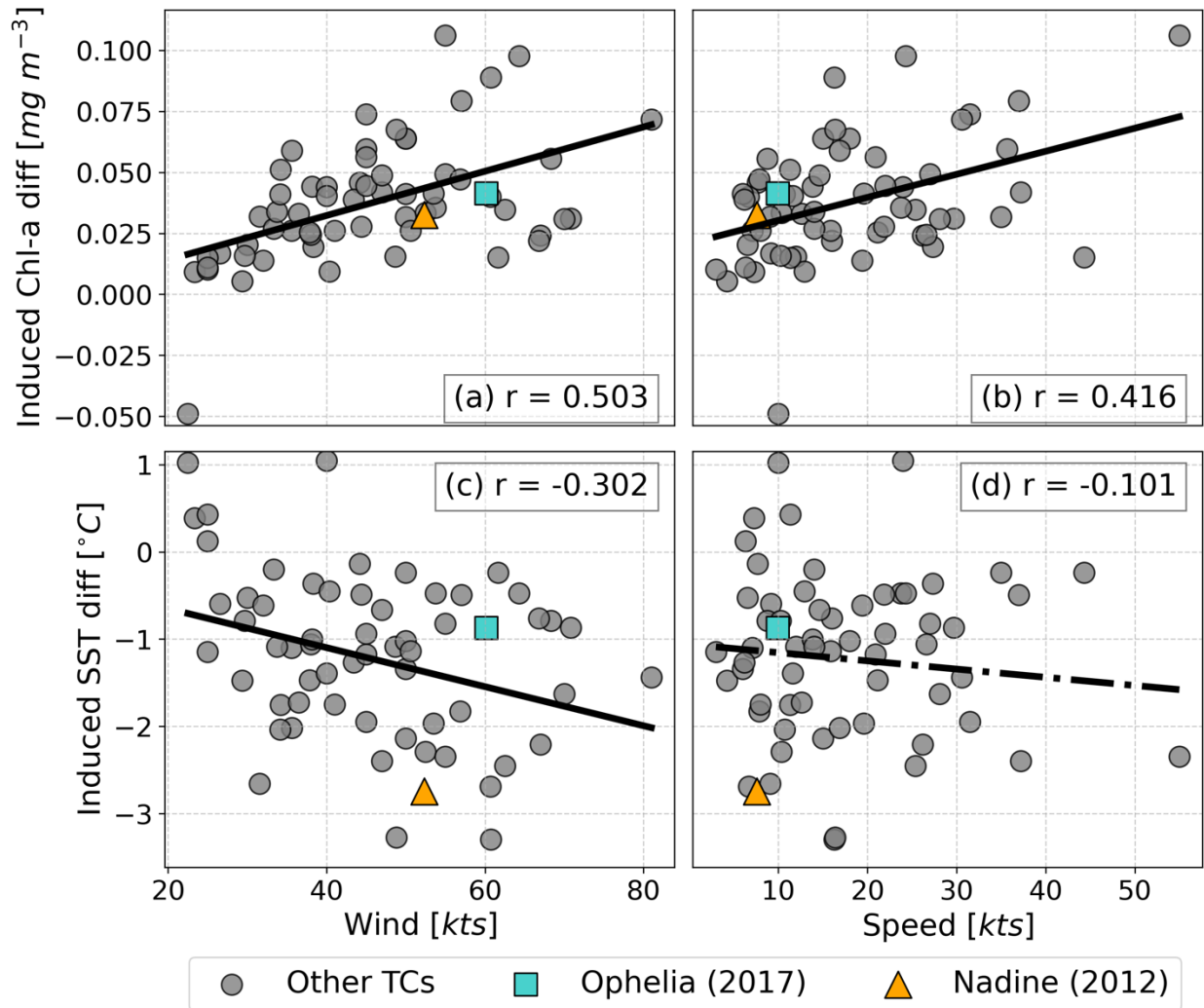
Figure 3 - Histograms for the: a) Total Chl-a and b) SST induced anomalies; c) Chl-a and d) SST induced anomalies after weak (blue) and powerful TCs (orange); e) Chl-a and f) SST induced anomalies after slow TCs (blue) and fast TCs (orange).

242 Each subplot histogram presents the respective population mean value ( $\mu$ ) in a dashed black line, and the zero value ~~on~~ in a  
 243 grey line.

244 To quantify these relations, Fig. 4 shows the storm-averaged induced anomalies compared to the averaged maximum  
 245 wind and average translation speed. The linear regression is also shown for each of the comparisons, with nearly all  
 246 results significant at the 95 % statistical level. According to these plots, only the translation speed in relation to the  
 247 SST induced anomalies (Figs. 4d) did not show a significant relation at the 95 % statistical confidence level (marked  
 248 by the dashed regression line). Regarding the mean wind (Figs. 4a and 4c), and therefore the TC's average intensity  
 249 within the Azores region, the linear regression showed ~~significantly high~~ significant values, upwards of 0.5 for Chl-a  
 250 and -0.3 for SST induced anomalies. In the case of Chl-a, like observed in Fig. 3, the relation is positive while with  
 251 SST this relation is negative. Considering the translation speed, the relation is equally positive and significant for  
 252 biological responses ( $r = 0.416$ ).



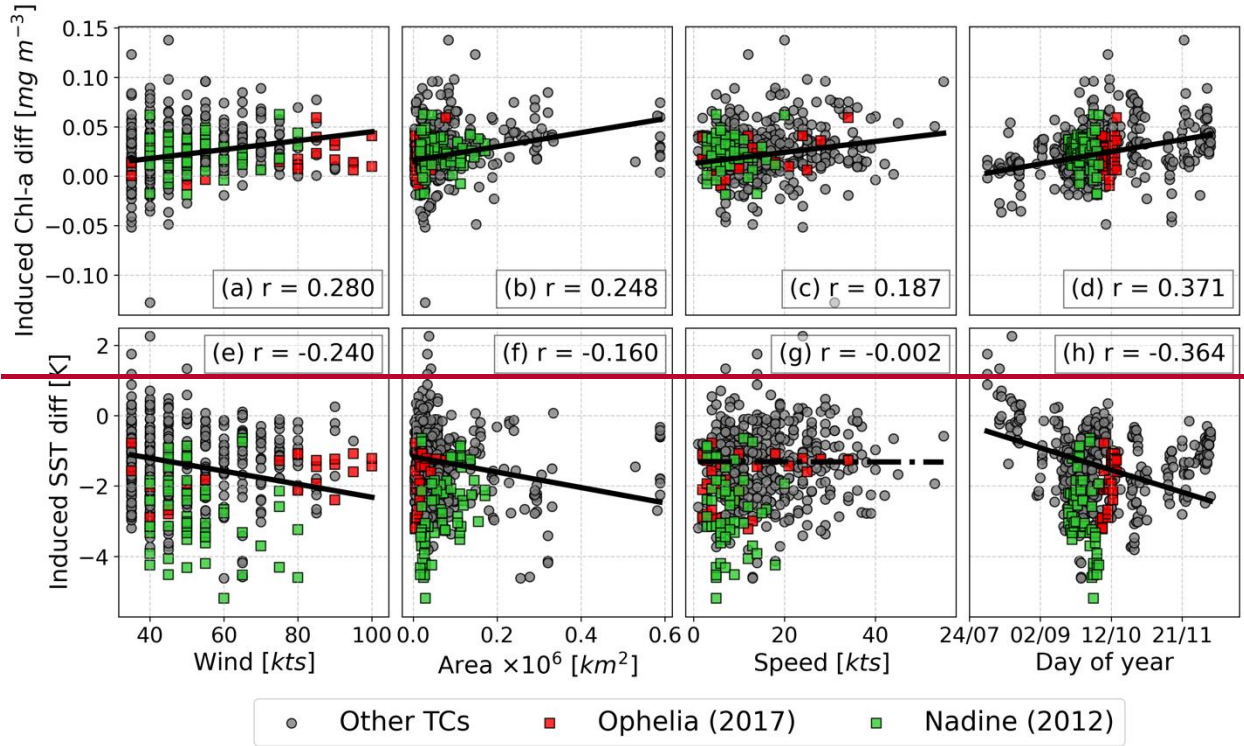
253



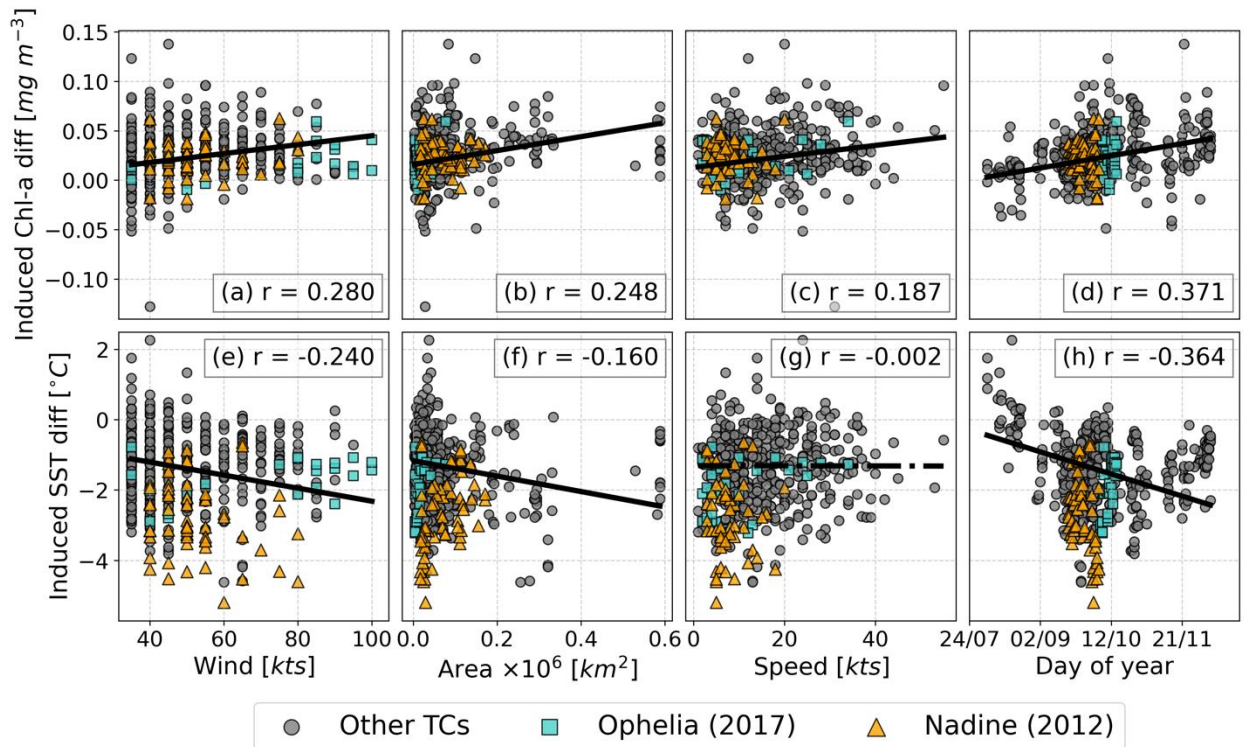
254

255 **Figure 4 - Linear regression of Chl-a (top panel) and SST (bottom panel) induced anomalies for each TC, respectively, when**  
 256 **compared with average winds in knots (left column); and average TC translation speed in knots (right column). In each**  
 257 **plot the Pearson R is presented, and the regression's significance is marked by the type of line used in the regression, with**  
 258 **a dashed line representing non-significant at a 95 % confidence level, and a solid line representing a regression significant**  
 259 **at the 95 % confidence level.**

260 Further analysis of other TC characteristics requires a different approach. Fig. 5 shows similar relations to Fig. 4, but  
 261 considering 6-hour observations instead of total TC mean values. This is made to account for the possible error that  
 262 averaging a whole TC may create since the cyclone's characteristics may change substantially along its lifetime. This  
 263 analysis, however, does not consider the possibility of superposition in pixels from observation to observation – i.e.,  
 264 from a TC that either moves slowly or whose track is more erratic, ending up covering the same area for several  
 265 hours/days. This caveat was not present in Fig. 4 since we considered the TC lifetime as a whole and could then  
 266 disregard the days of superposition. Using 6-hour observations, we can study several types of characteristics that  
 267 change between observations, such as the impact area or the time of season when it occurred, adding to the already  
 268 seen maximum wind speed and translation speed.



269



270

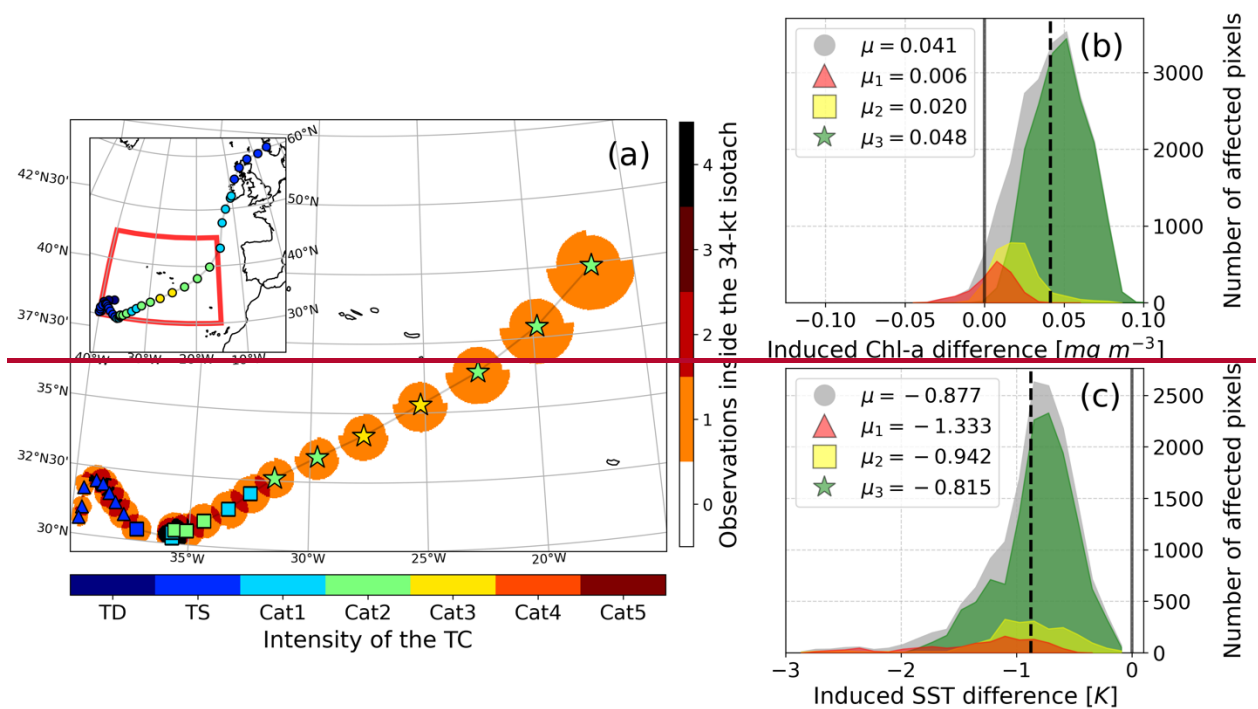
271 Figure 5 – Same as in Fig. 5 but considering individual 6-hour observations. Two columns are added: (b) and (f) with respect  
 272 to the area affected by that observation; and (d) and (h) with respect to the **season** **year** when that observation  
 273 occurred.

274 Considering then the maximum wind speed per observation (Fig. 5a and 5e), both variables are significantly related  
275 to this characteristic, which is expected considering the analysis made in Figs. 3 and 4. As previously noted in the  
276 form of histograms in Fig. 3, most observations show a positive impact regarding Chl-a and, especially for SST as  
277 most fall below zero, a negative change after a TC. The affected area (Figs. 5b and 5f) also presents a significant  
278 relation, although less intense than that observed with the maximum winds. However, it should be noted that this  
279 variable is linked to the mean winds, since more intense cyclones tend to be larger than less powerful ones, but also  
280 to the storm phase, since storms nearing their post-tropical transition tend to grow larger (Knaff et al., 2014).  
281 Translation speed is the less correlated variable from those studied (Fig. 5c and 5g), with only the biological response  
282 seeing a positive relation to this characteristic, agreeing with the previous results from Figs. 3 and 4. The time period  
283 in the season in which the TC occurs seems to also be important for the magnitude of the average induced anomaly  
284 seen in both variables (Figs. 5d and 5h) with late occurrences in the season showing greater responses respective to  
285 the signal of induced anomalies seen in Figs. 3a and 3b. Lastly, a geographical correlation was concluded not to be  
286 relevant for this study (not shown), as both variables were correlated with both latitude and longitude, and only  
287 ~~negligible and~~ non-significant relations were found.

288 The results presented so far in this study result from interpolated “cloud-free” data and should be quality assured to  
289 guarantee the integrity of the conclusions made previously. As mentioned in the *Data* section, CMEMS provides  
290 measures of uncertainty for the used Chl-a and SST datasets, ~~thus~~. Thus, we have explored these values at different  
291 periods as a first step in validating the quality of the data. Figure S1 shows the associated uncertainty with respect to  
292 the absolute observed values both for Chl-a (top panels) and SST (bottom panels) for three different periods  
293 surrounding a TC event (before, during, and after), and a randomly drawn sample of the same size as the data analysed  
294 in the other subplots. It becomes immediately clear from these plots the considerably different magnitude of  
295 uncertainty for this data, with Chl-a (Figs. S1a-d) ranging from 25 % to 45 % considering all moments, while SST  
296 (Fig. S1e-h) does not commonly surpass 0.4 % with a mean error around the 0.25 %. The randomly drawn sample of  
297 data gives a rough idea of the average uncertainty we can find in this dataset, with Chl-a (Fig. S1a) presenting values  
298 around 35 % and SST (Fig. S1e) around 0.25 %. Additionally, we should consider three distinct moments of analysis,  
299 namely before and after the TC passage, which corresponds to the data used to compute the induced anomalies, and  
300 during the TCs, which should be the moment with most cloud-cover over the studied regions. Looking first at Chl-a  
301 (Figs. S1b-d) we see the progression from near normal uncertainty before the TC (Fig. S1b) to an increase during TCs  
302 (Figs. S1c), ~~maybe~~ likely due to the ~~higher~~ larger cloud-covered area in ~~this~~ that situation, ~~after~~. After the storm (Fig.  
303 S1d) however, the uncertainty substantially decreases reaching values below the randomly drawn sample (around 30  
304 % compared to 35 %). For the SST (Figs. S1f-h), the associated uncertainty does not fluctuate substantially, constantly  
305 being below the 0.3 % mark. Additionally, ~~it is noticeable in both variables~~ the variation that has been identified  
306 before, with Chl-a increasing and the SST decreasing, is noticeable in both variables.

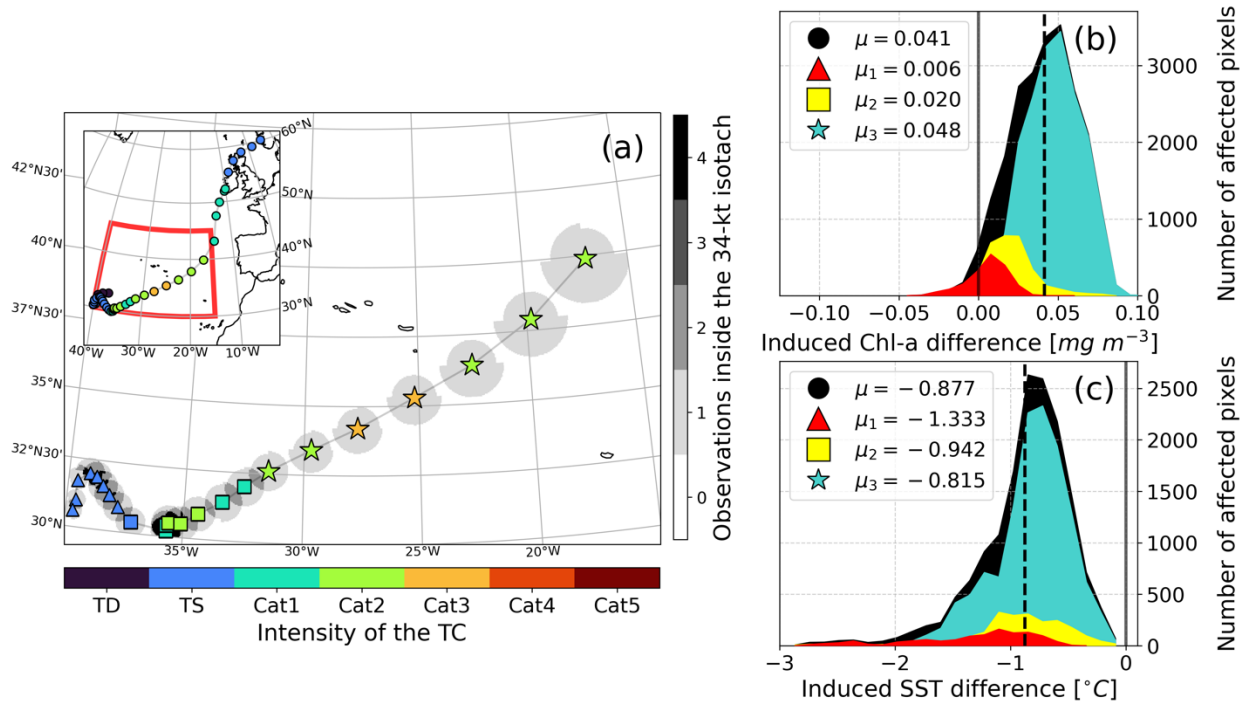
307 Visible in Figs. 4 and 5 are two case studies ~~are marked~~: Hurricane Ophelia in 2017 (~~red~~-squares) and Hurricane  
308 Nadine in 2012 (~~green squares~~ triangles). These case studies were chosen based on the presented characteristics,  
309 coupled with the amount of sampling data within the region. Hurricane Ophelia (2017) was chosen due to its large

310 intensity in the region (Red-squares, Fig. 4 and 5), reaching a category 3 intensity in the Saffir-Simpson hurricane  
 311 wind scale, something abnormal for the region (Lima *et al.*, 2021). The complete TC track can be seen in Fig. 6a  
 312 ~~inset~~inset. Besides the large intensity, Ophelia's genesis took place inside our study region which enabled us to study  
 313 different phases of the storm and its impacts on the ocean surface in the region. Even though hurricane Ophelia was  
 314 so intense, this storm impacted a very small area (Figs. 5b and 5f) particularly when compared with the other case  
 315 study, Hurricane Nadine (2012). Hurricane Nadine (Fig. 7a) was chosen due to its large sampling, relatively high  
 316 intensity (maximum category 1) and great impact area (second highest in this study, considering cumulative area of  
 317 impact). The large impacted area was amplified by the geometry of the storm's track (i.e., many overlaid observations).  
 318 Only the final stage of Hurricane Nadine was caught within the study region, producing an ideal case study to analyse  
 319 the impact of a less intense storm that heavily impacted a particular region due to its geometry.



320



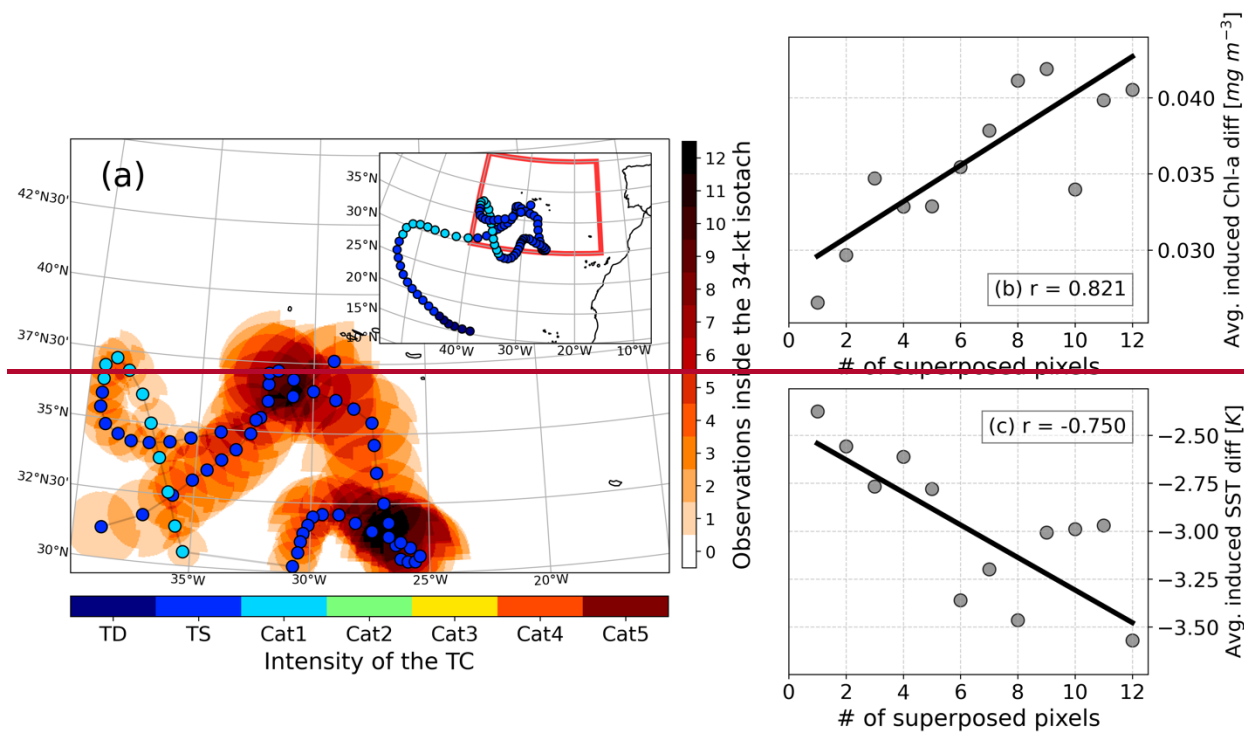


321

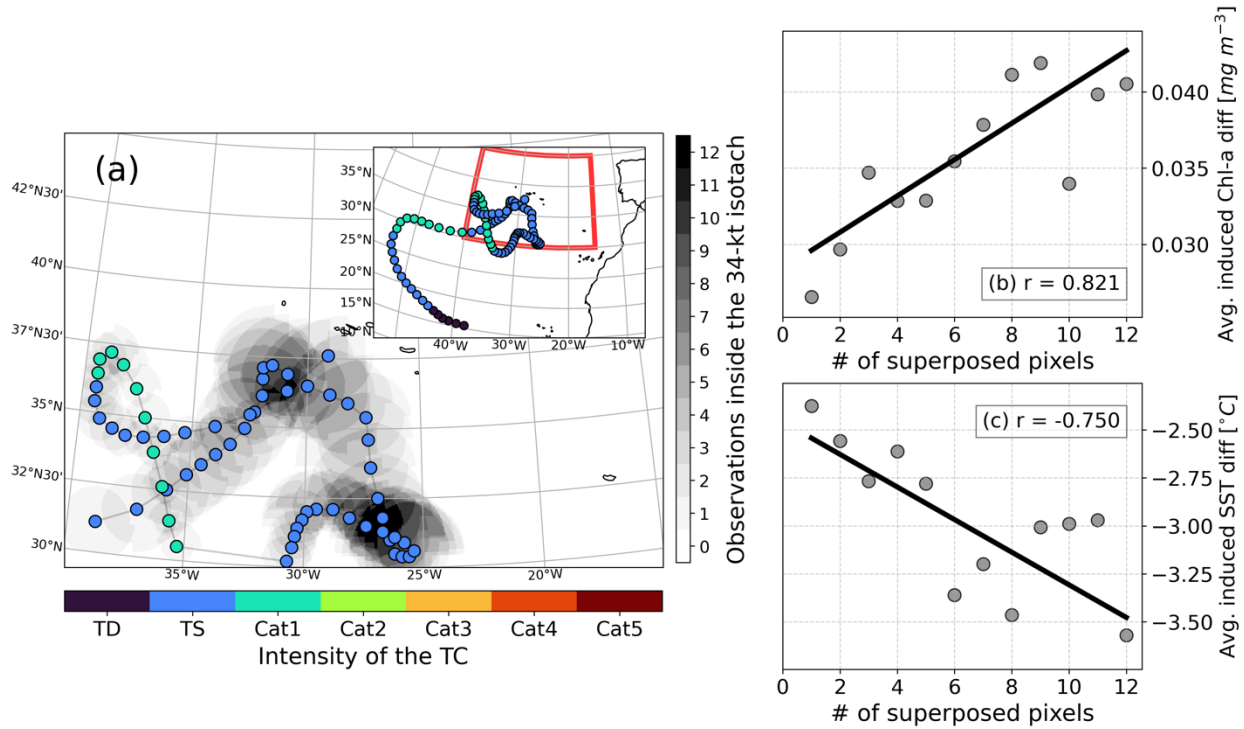
322 **Figure 6 - Case study for Hurricane Ophelia, in 2017, with its track on the left panel (scatter marker colour scheme**  
 323 **represents intensity as in Fig. 1), as well as the affected area around the cyclone (marked as the 34-kt isotach) with shading**  
 324 **according to the number of pixels overlapping. Inside, there is an inset with the full track and the region of study marked**  
 325 **with a red box. Ophelia track is divided in three phases: Histograms show induced Chl-a (b) and SST induced anomalies**  
 326 **(c), by phase of the storm (colours) and in total (grey/black). The phase of the storm is marked in (a) as triangles (genesis),**  
 327 **squares (maturing), and stars (mature) and correspond to the aforementioned-colours in (b) and (c).**

328 For the case study of Hurricane Ophelia (2017), three different phases of the storm were studied, corresponding  
 329 approximately to: cyclogenesis (Fig. 6a, triangles), maturing (Fig. 6a, squares), and mature hurricane (Fig. 6a, stars).  
 330 There are 23 total observations; the first two phases encompass 8 observations and the last one 7. Each of these phases  
 331 has its own histogram in Figs. 6b and 6c (shown in colours), for the induced Chl-a and SST TC-related anomalies,  
 332 respectively. The histograms are inserted in a larger one (in grey/black), representing the total induced anomalies  
 333 caused by Ophelia and therefore, the sum of all three phases will result in the bigger histogram. Regarding the Chl-a  
 334 induced anomalies (Fig. 6b), Ophelia seemed to have a higher impact towards the end of its track in the region of  
 335 study, when the storm had the highest intensity and the mean values of the induced anomalies increased along the  
 336 track. Even at the storm's genesis, the induced anomalies were mostly positive with a mean value of  $+0.006 \text{ mg m}^{-3}$   
 337 reaching  $+0.048 \text{ mg m}^{-3}$  in the most intense phase. In contrast, the SST induced anomalies (Fig. 6c) present the highest  
 338 mean response ( $-1.333 \text{ K}^{\circ}\text{C}$ ) at the initial phase. The SST induced anomaly is then seen decreasing as the storm goes  
 339 on, with the last phase weighing the most in the general distribution (as was seen for the Chl-a). The highest SST  
 340 impact of the storm during the initial phases may reflect that this is the phase of the storm with highest interaction  
 341 with the ocean, regarding thermodynamic exchanges (Emanuel, 2003).

342 As a further insight to Ophelia's interaction with the ocean surface, Fig. S3S2 shows the mean modulus of wind stress  
 343 on the surface, by day of analysis (Fig. S2a) and by Ophelia's 6-hour observations (Fig. S2b). Marked in both these  
 344 plots are the analysed periods in corresponding colours and marker type to Fig. 6, ~~these~~. These plots exceed the original  
 345 study region, in order to fully encompass the TCs entire lifetime. There is a significant relation between the increased  
 346 mean modulus of the wind stress and the evolution of the TC in time. This increase may be related to the increase in  
 347 the storm's intensity, ~~as~~. As Ophelia reaches its maximum intensity, so does the observed interaction with the ocean,  
 348 decreasing afterwards as the storm moves north-eastward and undergoes post-tropical transition. This observed  
 349 interaction with the ocean might be the reason for the maximum induced anomaly of Chl-a being observed at the end  
 350 of Ophelia's passage over the study region, inducing the mixing of the superficial layer.



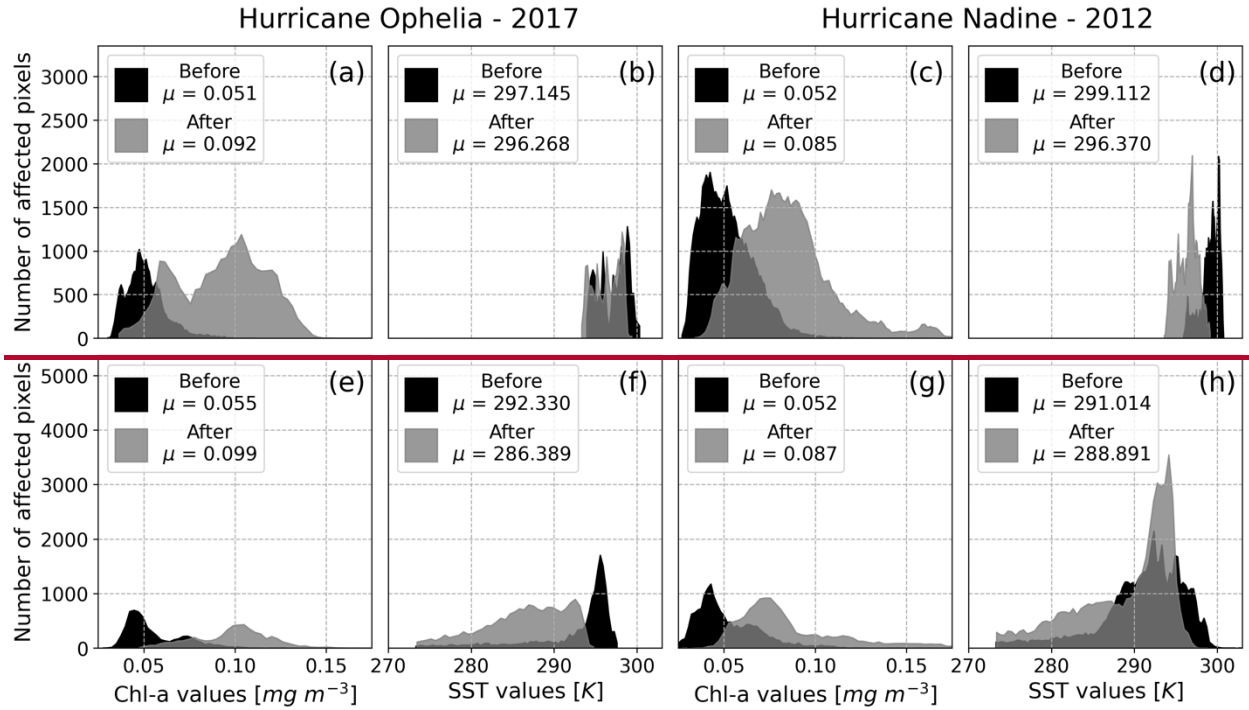
351



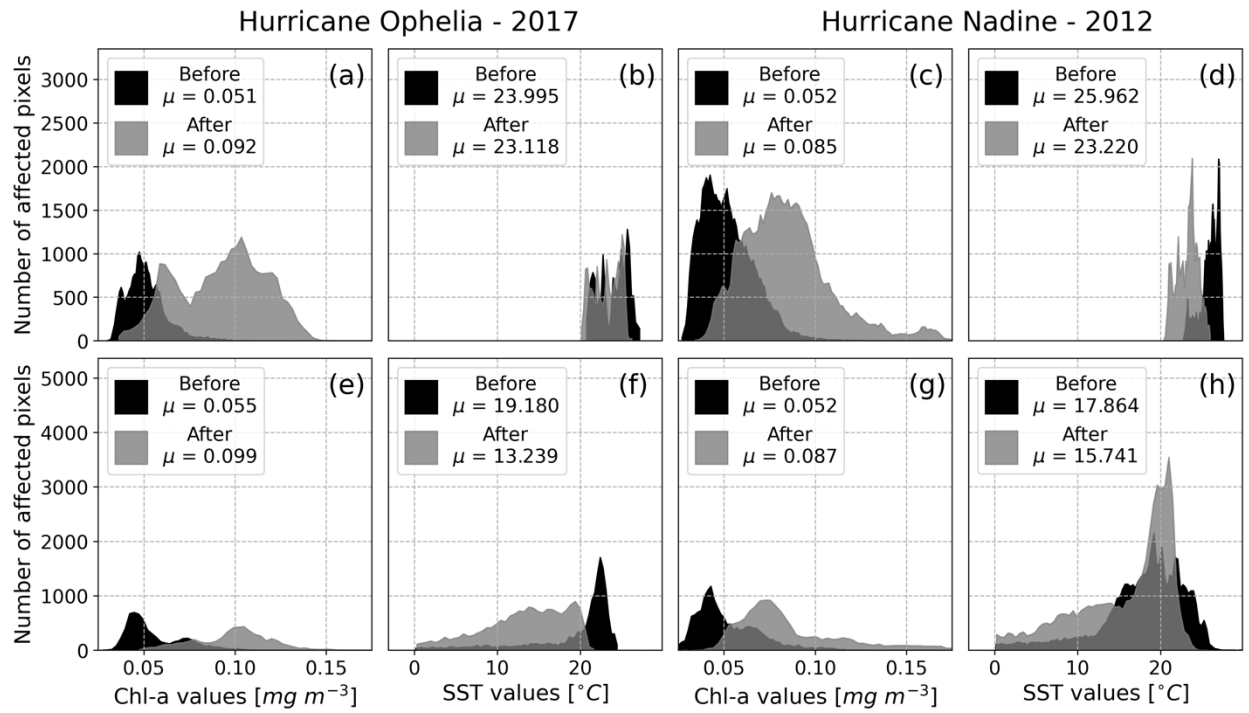
352

353 **Figure 7 - Case study for Hurricane Nadine, in 2012, with the left panel the same as in Fig. 6. For Nadine, plots (b) and (c)**  
 354 **pertain to the average induced Chl-a and SST induced anomalies, respectively, based on the amount of superposition**  
 355 **verified in each pixel.**

356 Hurricane Nadine's (2012) case study shows very different behaviour and impact during its lifetime to that of  
 357 Hurricane Ophelia. In this case, we present scatter plots of the averaged induced anomalies for the areas (Figs. 7b and  
 358 7c) corresponding to the superposition of pixels, i.e., the number of repeated observations inside the 34-kt isotach due  
 359 to storms track geometry (as seen in Fig. 7a). The conclusions drawn regarding the Chl-a and SST induced anomalies  
 360 are similar and significant in this case study: The more time the TC spent over a certain area the more this area became  
 361 affected by its passage, with large TC-related anomalies registered in both variables compared to less superposed ones  
 362 (over  $0.040 \text{ mg m}^{-3}$  and  $-3.500 \text{ }^{\circ}\text{C}$  for Chl-a and SST, respectively at 12 superposed pixels), and all cases being  
 363 positive (negative), for Chl-a (SST). It is possible to hypothesise that the translation speed also had a relevant role in  
 364 these results, with a slower TC (Nadine was one of the slowest TCs in this study, as seen by the closer observations  
 365 in Fig. 7a and by Figs. 4 and 5) spending more time over a region and therefore producing larger induced anomalies.



366



367

368 **Figure 8 – Comparison between interpolated “cloud-free” data (top row), and non-interpolated data (bottom row), for**  
 369 **Hurricanes Ophelia (2017) and Nadine (2012). Values for non-interpolated data were obtained with the same methodology**  
 370 **as the ones presented before and represent the exact same days of analysis. Mean values for each histogram are presented,**  
 371 **with black histograms representing the situation before the TC and the grey ones the situation after.**

372 For these two case studies, we considered an additional quality assessment exercise, by comparing the interpolated  
373 “cloud-free” data to similar non-interpolated datasets. Figure 8 shows the histograms obtained for Ophelia and Nadine  
374 for the situations before and after the TC, independently, since non-interpolated data cannot be correctly subtracted as  
375 corresponding pixels may not be available. Overall, and despite the different number of observations considered, the  
376 Chl-a presents the same average response between the different types of data for both TCs, with non-interpolated data  
377 having an observed mean increase of 0.044 mg m<sup>-3</sup> for Ophelia (Fig. 8e) compared to 0.041 mg m<sup>-3</sup> for interpolated  
378 data (Fig. 8a), with these values representing the difference in the mean values shown in Fig. 8. Likewise, non-  
379 interpolated data reveals an increase of 0.035 mg m<sup>-3</sup> for Nadine (Fig. 8g), compared to 0.033 mg m<sup>-3</sup> for interpolated  
380 data (Fig. 8c). Looking at the histograms, the shape of the data itself does not differ ~~too~~ much between the different  
381 types, with peaks more or less located over the same values and distributions ranging the same values. However, for  
382 the SST variable, despite both ~~TC's present~~ TCs presenting relatively similar decreases between both types of data,  
383 the non-interpolated data has a wider range of values, and the peaks do not correspond so closely. This, however, may  
384 be due to the process of data collation. In this process, some pixels are averaged with incorrect ones, resulting in  
385 unrealistic values in some areas. This can be identified by the unrealistic SST seen in Figs. 8f and 8h, with values that  
386 do not support TC development around 18-19°C and, so far as reaching 0°C. Nonetheless, interpolated SST data does  
387 show the less very low uncertainty as verified before ~~as the process of interpolating the data fixes this issue~~ (Fig. S1).

### 388 **Final remarks**

389 The current study provides the first general assessment of the bio-physical oceanic response to the passage of TCs in  
390 a relatively low cyclonic activity area such as the region near the Azores archipelago. It is important to stress the  
391 efficiency of identifying the precise timing and associated spatial impacts of all TCs using remotely sensed products  
392 that rely on interpolated areas to fill existing gaps due to cloud coverage or lack of satellite imagery.

393 Over the Azores region, ~~it was generally identified~~ the existence of a bio-physical response after the passage of a TC  
394 was identified from the analysis of Chl-a and SST datasets, which produced signatures of positive Chl-a and negative  
395 SST induced anomalies. This signature is more intense for the SST analysis, in which the passage of a TC results in  
396 nearly all observed pixels to have a negative (i.e., cooling) induced anomaly. On average, TCs produced positive  
397 induced anomalies in the order of 0.050 mg m<sup>-3</sup> regarding Chl-a and a mean SST cooling of 1.615 ~~K~~°C.

398 The more powerful TCs tend to produce more intense bio-physical oceanic responses, which agree with previous  
399 literature on the topic (Chacko, 2019; Price, 1981; Price et al., 1994). TC translation speed was also found to be  
400 associated with the induced anomalies, although the relationship was found to be positive and significant in the case  
401 of Chl-a while it was not significant at the 95 % statistical confidence level for SST. The impacted area was also found  
402 to be significantly linked to the oceanic response. However, the sensitivity to the impacted area can rise due to several  
403 other factors: slower TCs impact larger areas (due to track geometry); more intense TCs impact larger areas (Knaff et  
404 al., 2014); and TCs nearing post-tropical transition are generally larger (Knaff et al., 2014). These effects, either  
405 individually or combined, can affect the induced anomalies at different levels. Additionally, the oceanic response was  
406 found to be ~~increased~~ larger later in the season, with significant relation in both variables, ~~this~~. This may be due to the

407 seasonal variability ~~of the variables themselves~~itself, as the normal climatological values for that time of the year ~~is~~  
408 ~~exceeded~~are not seen during exceptional TC conditions (e.g. SST is usually colder but TC prone conditions require  
409 it to be higher) (Amorim et al., 2017; Lima et al., 2021) and the oceanic response may help the impacted area return  
410 to ~~expected~~-values closer to the climatology, in both variables, in respect to that time of the year.

411 Two particular case studies were evaluated in further detail concerning hurricanes Ophelia (2017) and Nadine (2012).  
412 Hurricane Ophelia was a particular case as it corresponds to the only major hurricane in this study region and had  
413 almost its entire track inside this area. Ophelia showed strong induced anomalies for both Chl-a and SST variables.  
414 Regarding Chl-a, Ophelia had a stronger impact towards the end of its track within the region, revealing that its  
415 intensity played a key role in inducing Chl-a TC-related anomalies, with the mean modulus of wind stress revealing a  
416 positive and significative relation to the evolution of the storm and therefore its intensity. On the other hand, Ophelia  
417 had a stronger impact on the SST in its cyclogenesis, probably related to ocean-atmosphere thermodynamic exchanges  
418 during its maturing. Hurricane Nadine, one of the slowest TCs in this study, showed more prominent induced  
419 anomalies, especially regarding SST. In this case, considering the low translational speed of Nadine, the objective was  
420 to study the impact that consecutive overlaid observations had on the induced anomalies. It is evident through this  
421 analysis that the impact increases with the number of superposed observations, implying that Nadine's slow translation  
422 speed and particular track geometry played a key role in creating such TC-related anomalies.

423 This study allowed for both the quality control of the remotely sensed “cloud-free” Chl-a and SST multi-sensor  
424 products by comparing them to similar non-interpolated products, and in the sense that it identified expected changes  
425 in the variables in areas covered by TC clouds and established crucial relations with some principal TC aspects. Future  
426 studies should aim to understand the inherent physical mechanisms that affect the ocean during and after the passage  
427 of a TC to better comprehend the associated induced anomalies.

#### 428 **Code and Data availability**

429 All code and raw data used to support the conclusion of this article will be made available by the authors, without  
430 undue reservation.

#### 431 **Acknowledgements**

432 Research by Miguel M. Lima was supported by the Portuguese Science Foundation (FCT) through the project  
433 “DiscoverAZORES”, PTDC/CTA-AMB/28511/2017. The authors would like to thank the anonymous reviewers for  
434 their thoughtful comments, suggestions, and efforts towards improving this work.

#### 435 **Author Contribution**

436 Miguel M. Lima: Conceptualization, methodology, software, validation, formal analysis, investigation, writing –  
437 original draft, review and editing. Célia M. Gouveia: Validation, supervision, writing – review and editing. Ricardo  
438 M. Trigo: Validation, supervision, writing – review and editing, funding acquisition.

439 **Declaration of Interests**

440 The authors declare that they have no known competing financial interests or personal relationships that could have  
441 appeared to influence the work reported in this paper.

442 **References**

- 443 Amorim, P., Perán, A. D., Pham, C. K., Juliano, M., Cardigos, F., Tempera, F., and Morato, T.: Overview of the  
444 ocean climatology and its variability in the Azores region of the North Atlantic including environmental  
445 characteristics at the seabed, *Frontiers in Marine Science*, 4, 56, doi:10.3389/fmars.2017.00056, 2017.
- 446 Baatsen, M., Haarsma, R. J., Van Delden, A. J., and de Vries, H.: Severe Autumn Storms in Future Western Europe  
447 with a Warmer Atlantic Ocean, *Clim. Dyn*, 45 (3-4), 949–964, doi:10.1007/s00382-014-2329-8, 2015.
- 448 Caldeira, R., and Reis, J. C.: The Azores confluence zone. *Frontiers in Marine Science*, 4, 37,  
449 doi:10.3389/fmars.2017.00037, 2017.
- 450 Chen, S., Elsberry, R. L., and Harr, P. A.: Modelling interaction of a tropical cyclone with its cold wake, *J. Atmos.*  
451 *Sci.*, 74(12), 3981-4001, doi:10.1175/JAS-D-16-0246.1, 2017.
- 452 Chacko, N.: Differential chlorophyll blooms induced by tropical cyclones and their relation to cyclone  
453 characteristics and ocean pre-conditions in the Indian Ocean. *J. Earth Syst. Sci.*, 128(7), 1-11. doi:10.1007/s12040-  
454 019-1207-5, 2019.
- 455 CMEMS: ESA SST CCI and C3S reprocessed sea surface temperature analyses. Retrieved from  
456 [https://resources.marine.copernicus.eu/?option=com\\_csw&view=details&product\\_id=SST\\_GLO\\_SST\\_L4](https://resources.marine.copernicus.eu/?option=com_csw&view=details&product_id=SST_GLO_SST_L4)  
457 [REP OBSERVATIONS 010 024](https://resources.marine.copernicus.eu/?option=com_csw&view=details&product_id=SST_GLO_SST_L4), 2021a.
- 458 CMEMS: Global ocean chlorophyll, PP and PFT (copernicus-globcolour) from satellite observations: Monthly and  
459 daily interpolated (reprocessed from 1997). Retrieved from  
460 [https://resources.marine.copernicus.eu/?option=com\\_csw&view=details&product\\_id=OCEANCOLOUR\\_GLO\\_CH](https://resources.marine.copernicus.eu/?option=com_csw&view=details&product_id=OCEANCOLOUR_GLO_CH)  
461 [L L4 REP OBSERVATIONS 009 082](https://resources.marine.copernicus.eu/?option=com_csw&view=details&product_id=OCEANCOLOUR_GLO_CH), 2021b.
- 462 Dickey, T., Frye, D., McNeil, J., Manov, D., Nelson, N., Sigurdson, D., ... and Johnson, R.: Upper-ocean  
463 temperature response to Hurricane Felix as measured by the Bermuda Testbed Mooring, *Mon. Weather Rev.*,  
464 126(5), 1195-1201, doi:10.1175/1520-0493(1998)126<1195:UOTRTH>2.0.CO;2, 1998.
- 465 Donlon, C. J., Martin, M., Stark, J., Roberts-Jones, J., Fiedler, E., and Wimmer, W.: The operational sea surface  
466 temperature and sea ice analysis (OSTIA) system, *Proc. SPIE*, 116, 140-158, doi:10.1016/j.rse.2010.10.017, 2012.
- 467 Emanuel, K., Tropical Cyclones. *Annu. Rev. Earth Pl. Sc.*, 31 (1), 75–104,  
468 doi:10.1146/annurev.earth.31.100901.141259, 2003.

469 Garnesson, P., Mangin, A., Fanton d'Andon, O., Demaria, J., and Bretagnon, M.: The CMEMS GlobColour  
470 chlorophyll a product based on satellite observation: multi-sensor merging and flagging strategies, *Ocean Sci.*,  
471 15(3), 819-830, doi:10.5194/os-15-819-2019, 2019.

472 Good, S., Fiedler, E., Mao, C., Martin, M. J., Maycock, A., Reid, R., ... and Worsfold, M.: The current configuration  
473 of the OSTIA system for operational production of foundation sea surface temperature and ice concentration  
474 analyses, *Remote Sens.-Basel.*, 12(4), 720, doi:10.3390/rs12040720, 2020.

475 Haarsma, R. J., Hazeleger, W., Severijns, C., de Vries, H., Sterl, A., Bintanja, R., ..., and van den Brink, H. W.:  
476 More Hurricanes to Hit Western Europe Due to Global Warming, *Geophys. Res. Lett.*, 40, 1783–1788,  
477 doi:10.1002/grl.50360, 2013.

478 Hart, R. E., and Evans, J. L.: A climatology of the extratropical transition of Atlantic tropical cyclones, *J. Climate*,  
479 14(4), 546-564, doi:10.1175/1520-0442(2001)014<0546:ACOTET>2.0.CO;2, 2001.

480 Holton, J. R., and Hakim, G. J., *An Introduction to Dynamic Meteorology*, 5th ed., Vol. 88. San Diego, CA:  
481 Academic Press, Elsevier, doi:10.1119/1.1987371, 2012.

482 Kawai, Y., and Wada, A.: Detection of cyclone-induced rapid increases in chlorophyll-a with sea surface cooling in  
483 the northwestern Pacific Ocean from a MODIS/SeaWiFS merged satellite chlorophyll product, *Int. J. Remote Sens.*,  
484 32(24), 9455-9471, doi:10.1080/01431161.2011.562252, 2011.

485 Knaff, J. A., Longmore, S. P., and Molenaar, D. A.: An objective satellite-based tropical cyclone size climatology, *J.*  
486 *Climate*, 27(1), 455-476, doi:10.1175/JCLI-D-13-00096.1, 2014.

487 Knapp, K. R., Kruk, M. C., Levinson, D. H., Diamond, H. J., and Neumann, C. J.: The International Best Track  
488 Archive for Climate Stewardship (IBTrACS), *B. Am. Meteorol. Soc.*, 91 (3), 363–376,  
489 doi:10.1175/2009BAMS2755.1, 2010.

490 Kossin, J. P., Knapp, K. R., Olander, T. L., and Velden, C. S.: Global Increase in Major Tropical Cyclone  
491 Exceedance Probability over the Past Four Decades, *P. Natl. A. Sci USA*, 117 (22), 11975–11980,  
492 doi:10.1073/pnas.1920849117, 2020.

493 Krasnopolsky, V., Nadiga, S., Mehra, A., Bayler, E., and Behringer, D.: Neural networks technique for filling gaps  
494 in satellite measurements: Application to ocean color observations, *Comput. Intel. Neurosc.*, 2016, 29,  
495 doi:10.1155/2016/6156513, 2016.

496 Lavergne, T., Sørensen, A. M., Kern, S., Tonboe, R., Notz, D., Aaboe, S., ... and Pedersen, L. T.: Version 2 of the  
497 EUMETSAT OSI SAF and ESA CCI sea-ice concentration climate data records, *The Cryosphere*, 13(1), 49-78,  
498 doi:10.5194/tc-13-49-2019, 2019.

499 Lima, M. M. , Hurduc, A., Ramos, A. M. and Trigo, R. M.: The Increasing Frequency of Tropical Cyclones in the  
500 Northeastern Atlantic Sector, *Front. Earth Sci.*, 9:745115, doi: 10.3389/feart.2021.745115, 2021.



501 Liu, X., Wang, M., and Shi, W.: A study of a Hurricane Katrina–induced phytoplankton bloom using satellite  
502 observations and model simulations, *J. Geophys. Res-Oceans*, 114(C3), doi:10.1029/2008JC004934, 2009.

503 Maneesha, K., Murty, V. S. N., Ravichandran, M., Lee, T., Yu, W., and McPhaden, M. J.: Upper ocean variability in  
504 the Bay of Bengal during the tropical cyclones Nargis and Laila, *Prog. Oceanogr.*, 106, 49-61,  
505 doi:10.1016/j.pocean.2012.06.006, 2012.

506 Merchant, C. J., Le Borgne, P., Roquet, H., and Legendre, G.: Extended optimal estimation techniques for sea  
507 surface temperature from the Spinning Enhanced Visible and Infra-Red Imager (SEVIRI), *Proc. SPIE*, 131, 287-297,  
508 doi:10.1016/j.rse.2012.12.019, 2013.

509 Pan, J., Huang, L., Devlin, A. T., and Lin, H.: Quantification of typhoon-induced phytoplankton blooms using  
510 satellite multi-sensor data. *Remote Sens-Basel*, 10(2), 318, doi:10.3390/rs10020318, 2018.

511 Pearce, R. P.: The physics of hurricanes. *Phys. Technol.*, 18(5), 215, 1987.

512 Price, J. F.: Upper ocean response to a hurricane. *J. Phys. Oceanogr.*, 11(2), 153-175, doi:10.1175/1520-  
513 0485(1981)011<0153:UORTAH>2.0.CO;2, 1981.

514 Price, J. F., Sanford, T. B., and Forristall, G. Z.: Forced stage response to a moving hurricane. *J. Phys. Oceanogr.*,  
515 24(2), 233-260, doi:10.1175/1520-0485(1994)024<0233:FSRTAM>2.0.CO;2, 1994.

516 Ramsay, H.: *The Global Climatology of Tropical Cyclones*. Oxford Research Encyclopedia of Natural Hazard  
517 Science. Victoria, Australia: Oxford University Press, doi:10.1093/acrefore/9780199389407.013.79, 2017.

518 Saha, K., Zhao, X., Zhang, H., Casey, K. S., Zhang, D., Baker-Yeboah, S., ... and Relph, J. M.: AVHRR Pathfinder  
519 version 5.3 level 3 collated (L3C) global 4km sea surface temperature for 1981-Present, NOAA National Centers for  
520 Environmental Information, dataset, doi:10.7289/v52j68xx, 2018.

521 Sathyendranath, S., Brewin, R. J. W., Brockmann, C., Brotas, V., Calton, B., Chuprin, A., ... and Platt, T.: An  
522 ocean-colour time series for use in climate studies: the experience of the Ocean-Colour Climate Change Initiative  
523 (OC-CCI), *AH S. Sens.*, 19(19), 4285, doi:10.3390/s19194285, 2019.

524 Sathyendranath, S., Jackson, T., Brockmann, C., Brotas, V.; Calton, B., Chuprin, A., ... and Platt, T.: ESA Ocean  
525 Colour Climate Change Initiative (Ocean\_Colour\_cci): Version 5.0 Data, NERC EDS Centre for Environmental  
526 Data Analysis, 19 May 2021, doi:10.5285/1dbe7a109c0244aad713e078fd3059a, 2021.

527 Saulquin, B., Gohin, F., and Fanton d'Andon, O.: Interpolated fields of satellite-derived multi-algorithm  
528 chlorophyll-a estimates at global and European scales in the frame of the European Copernicus-Marine Environment  
529 Monitoring Service. *J. of Oper. Oceanogr.*, 12(1), 47-57, doi:10.1080/1755876X.2018.1552358, 2019.

530 Shropshire, T., Li, Y., and He, R.: Storm impact on sea surface temperature and chlorophyll a in the Gulf of Mexico  
531 and Sargasso Sea based on daily cloud-free satellite data reconstructions, *Geophys. Res. Letters*, 43(23), 12-199,  
532 doi:10.1002/2016GL071178, 2016.

- 533 Subrahmanyam, B., Rao, K. H., Srinivasa Rao, N., Murty, V. S. N., and Sharp, R. J.: Influence of a tropical cyclone  
534 on chlorophyll-a concentration in the Arabian Sea, *Geophys. Res. Letters*, 29(22), 22-1,  
535 doi:10.1029/2002GL015892, 2002.
- 536 Taylor, H. T., Ward, B., Willis, M., and Zaleski, W.: The saffir-simpson hurricane wind scale. Atmospheric  
537 Administration: Washington, DC, USA., 2010.
- 538 Walker, N. D., Leben, R. R., and Balasubramanian, S.: Hurricane-forced upwelling and chlorophyll-a enhancement  
539 within cold-core cyclones in the Gulf of Mexico, *Geophys. Res. Letters*, 32(18), doi:10.1029/2005GL023716, 2005.
- 540 Zhang, J., Lin, Y., Chavas, D. R., and Mei, W.: Tropical cyclone cold wake size and its applications to power  
541 dissipation and ocean heat uptake estimates. *Geophys. Res. Letters*, 46(16), 10177-10185,  
542 doi:10.1029/2019GL083783, 2019.
- 543 Zheng, Z. W., Ho, C. R., and Kuo, N. J.: Importance of pre-existing oceanic conditions to upper ocean response  
544 induced by Super Typhoon Hai-Tang. *Geophys. Res. Letters*, 35(20), doi:10.1029/2008GL035524, 2008.